ELSEVIER

Polymer 41 (2000) 311–321

polymer

Phase distribution in polyethylene versus temperature probed by solid-state proton NMR free induction decay

P.E. Kristiansen[a], E.W. Hansen[b,*], B. Pedersen[a]

[a]*Department of Chemistry, University of Oslo, P.O. Box 1033, Blindern, 0315 Oslo, Norway*
[b]*SINTEF Applied Chemistry, P.O. Box 124, Blindern, 0314 Oslo, Norway*

Received 3 July 1998; received in revised form 18 December 1998; accepted 14 January 1999

Abstract

The change in the solid-state proton NMR Free Induction Decay signal of a polyethylene sample while heating from 360 to approximately 400 K was investigated. The crystallinity, as determined by model fit, decreases approximately linearly with increasing temperature up to 393 K. At higher temperature, the crystallinity decreases faster with increasing temperature. Within the temperature region investigated, three different "phases" are identified. The change in the relative distribution of these phases versus temperature is explained quantitatively by a phase-equilibrium model. Spin–spin relaxation time measurements and second moment calculations are presented, which gives information about molecular motion within these phases.

Keywords: Free induction decay; Spin–spin relaxation; Crystalline phase

1. Introduction

Use of NMR spectroscopy to derive structural information on polymers has received considerable attention during the last four decades, of which a few publications are cited in the list of references [1–7]. Also, NMR has been shown to give useful information on the morphology of semi-crystalline polyolefins [8].

Dadayli et al. [9] and Hansen et al. [10] have recently reported on the crystallinity of polyolefins [polypropylene and polyethylene (PE)] from solid-state proton NMR Free Induction Decay (FID) analysis and showed that the derived crystallinity is in excellent agreement with crystallinity obtained by density measurements and Differential Scanning Calorimetry (DSC) measurements. In particular, we showed that the crystallinity obtained from conventional FT-NMR spectral analysis was underestimated by approximately 8% (on an absolute scale) for a sample with crystallinity of 68% (as determined by NMR FID analysis) [10]. This systematic discrepancy originates from the obligatory blanking time of the receiver introduced to avoid breakthrough of rf-pulses.

Also, pre-melting and softening are processes of significant impact on the physical characteristics of polymers [11] and have been investigated by calorimetric measurements [12], rheological techniques [11] and NMR measurements [13,14].

Based on recently published work [10], we found it was of interest to apply this solid-state proton NMR "FID analysis technique" to characterize a pre-melted PE sample by monitoring the crystallinity and potential phase changes within the polymer versus temperature, in situ. Also, molecular motional characteristics of the different phases as well as the mathematical-physical model(s) used to quantify the FID will be addressed. Quantification of the distribution of phases versus temperature will be another subject of interest in this report.

In short, the main object of this presentation is to emphasize the potential use of the NMR FID analysis technique to characterize PEs and other polyolefins.

2. Experimental

2.1. Material

The single PE sample investigated in this work was received from Borealis AS. The degree of branching was determined by sampling a carbon NMR spectrum of the PE sample dissolved in orthodichlorobenzene (ODCB) at 403 K.

The solid PE sample was initially melted at 428 K within the NMR magnet and then cooled in a flow of nitrogen

* Corresponding author. Fax: + 47-2206-7350.

0032-3861/00/$ - see front matter
PII: S0032-3861(99)00091-9

(300 K) down to 368 K at a cooling rate of approximately 20 K/min. The subsequent cooling down to room temperature took approximately 7 min, corresponding to a cooling rate of approximately 10 K/min. The sample was then temperature equilibrated for 30 min at room temperature.

The sample was heated to the actual temperature and the FID signal acquired in the temperature range 360–400 K. Before acquiring any FID, the sample was allowed to temperature equilibrate for approximately 10 min.

3. NMR

All NMR measurements were performed on a Bruker DMX 200 AVANCE instrument operating at 200 MHz proton resonance frequency. A high-power ^{1}H NMR probe capable of producing 90° radio frequency (rf) pulses of approximately 1.5 μs was used. The FID was sampled every 0.2 μs. To avoid pulse breakthrough, a receiver blanking time ("dead time") of 2 μs was applied. Four scans were acquired in each experiment with a repetition time of 20 s between each scan. This repetition time is much longer than five times the longer spin–lattice relaxation time T_1 (<1.5 s) of the methylene protons and ensures quantitative sampling of the FID. The actual phase parameters were adjusted manually to give a pure absorption spectrum in order to ensure that only the real part of the FID is sampled [15].

Each FID was sampled from 2 μs up to 4.4 ms, corresponding to approximately 22 K of data points. Before transforming the data to a PC for post processing, the data matrix was reduced in size by selecting all sampled data points from 2 to 42 μs (200 points), and each 44 data points from 42 μs up (500 data points). This particular reduction and selection of data points, from 22 to 0.7 K, was favored by visual inspection of all sampled FIDs, simultaneously. The reason for performing such a data reduction or filtering, was to speed up the subsequent calculation (on a PC) when using the program "solver" in Microsoft Excel.

The temperature within the probe was calibrated by use of a NMR thermometer of ethylene glycol and controlled by a Bruker B-VT unit, manufactured by Oxford Instruments Ltd. The actual temperature was estimated to be stable and accurate to about ±1 K.

For the high-resolution, liquid state NMR experiment, the PE sample was dissolved in ODCB in a 5 mm outer diameter NMR tube (approximately 12.5 wt.% of polymer in solution) and saturated with nitrogen gas before being sealed. The polymer was dissolved at 423 K for 30 min before a proton decoupled ^{13}C spectrum was acquired at 403 K on a Varian VXR 300 NMR spectrometer, operating at 75 MHz carbon resonance frequency. A π/2-pulse was applied with an acquisition time of 1s. The pulse repetition time was fixed at 60 s and the sweep width set to 18 kHz using 64 K data points. The intensity (area) of each peak was determined by mathematical deconvolution, i.e. fitting the resonance peak to a Lorenzian function by a non-linear least squares procedure, which gives an optimum value of peak position (chemical shift) and peak intensity (area).

4. Theoretical outline

4.1. Crystalline phase

From a NMR point of view, PE represents a rather "simple" polymer system in which the two proton nuclei of each methylene group constitute a strong dipole–dipole coupled two-spin system. As a result of the weaker dipole–dipole coupling between protons on different methylene groups, the absorption line shape function of the protons in PE can be considered, to a good approximation, to arise from a Gaussian broadened two-spin interaction, where the broadening is being caused by other neighbors. Pake [16] derived an analytical expression for such an absorption spectrum of coupled spin 1/2 nuclei. However, owing to the inherent NMR dilemma related to rf-pulse breakthrough [17], the theoretical Pake function cannot be fitted directly to the frequency spectrum. Rather, we need to obtain the inverse Fourier Transform of the Pake expression, which will represent the observed signal intensity in the time domain. Look and coworkers [18] presented an analytical solution to this enigma, which has been used recently by Hansen et al. [10]

$$P(t) = \sqrt{\frac{\pi}{6}}\exp\left[-\frac{1}{2}\beta^2 t^2\right] \times\left\{\frac{\cos\alpha t}{\sqrt{\alpha t}}\mathrm{C}\left[\sqrt{\frac{6\alpha t}{\pi}}\right] + \frac{\sin\alpha t}{\sqrt{\alpha t}}\mathrm{S}\left[\sqrt{\frac{6\alpha t}{\pi}}\right]\right\}, \quad (1a)$$

where $P(t)$ defines the normalized time dependent FID signal and $\mathrm{C}(x)$ and $\mathrm{S}(x)$ are the so-called Fresnel functions which are defined as simple integral equations [19]. The parameter α is related to the distance, $R_{\mathrm{H-H}}$, between the two nearest neighbour protons of the methylene group

$$\alpha = \frac{\mu_0}{4\pi}\frac{3}{4}\frac{\gamma^2\hbar}{R^3_{\mathrm{H-H}}}, \quad (1b)$$

where γ is the nuclear gyromagnetic ratio and $\hbar$ is Planck's constant, and β represents the width of the Gaussian broadening function, which takes account of dipole–dipole interactions between protons on different methylene groups. In order to apply Eq. (1) as a fitting function, a more tractable form of the Fresnel functions is needed. The following approximations have been used [19]:

$$\mathrm{C}(x) = \frac{1}{2} + f(x)\sin\left[\frac{\pi}{2}x^2\right] - g(x)\cos\left[\frac{\pi}{2}x^2\right], \quad (1c)$$

$$\mathrm{S}(x) = \frac{1}{2} + f(x)\cos\left[\frac{\pi}{2}x^2\right] - g(x)\sin\left[\frac{\pi}{2}x^2\right], \quad (1d)$$

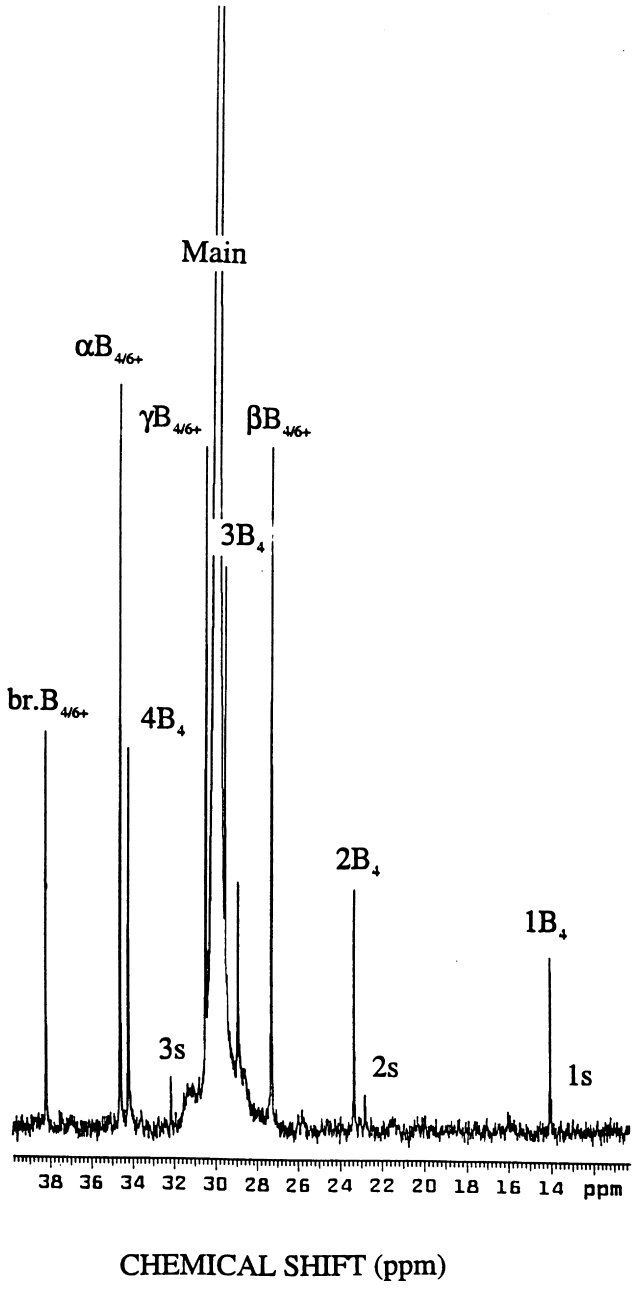

Fig. 1. ^{13}C-{^{1}H} n.m.r. spectrum of a 12.5 wt.% PE sample dissolved in ODCB. Spectrum acquired at 403 K. Main peak is set at $\delta = 29.980$ ppm.

where

$$f(x) = \frac{1 + 0.926x}{2 + 1.792x + 3.104x^2} + \varepsilon(x), \tag{1e}$$

$$g(x) = \frac{1}{2 + 4.142x + 3.492x^2 + 6.670x^3} + \varepsilon(x). \tag{1f}$$

The absolute error, $\varepsilon(x)$, in these approximations is less than 2×10^{-3}.

Dadayli et al. [9] have used an approximate form of Eq. (1), which is defined by a Gaussian-broadened sinc function

$$A(t) = \frac{\sin(\omega t)}{\omega t} \exp\left(-\left(\frac{t}{T_2}\right)^2\right). \tag{2}$$

Eq. (2) was first suggested and used by Abragam as a phenomenological expression of the [19] FID signal of CaF_2, and is—in this work—simply denoted an "Abragamian" [20]. It has been found to be a good representation of the FID from other regular, crystalline lattices [9]. Both of these models, Eqs. (1) and (2), will be applied in the present work when discussing the crystallinity of PE.

4.2. Amorphous phase

In contrast to the crystalline phase of PE, the amorphous phase is evidenced by an increased fluctuation in the molecular mobility, which is expected to modify the shape of the NMR spectrum. Brereton et al. [21,22] have derived an exact, theoretical expression for the FID of a dynamic scale invariant polymer chain governed by a single relaxation time. This type of function was shown to give a satisfactory representation of the FID of amorphous PE above its glass transition temperature, T_g. Also, this same function was shown to give a reasonable reproduction of the FID from PE melts over a range of temperatures, and was successfully applied by us in a recent investigation of PE at room temperature [10]. The analytical form of the "Brereton" function is rather complex and will not be discussed further in this work.

Dadayli et al. [9] have pointed out that the rather complex Brereton function can be well approximated by the sum of a Weibullian function, $W(t)$, and one or two exponential functions

$$W(t) = \exp\left[-(t/T_{2c})^n\right]. \tag{3}$$

The normalized Weibullian function ranges between a pure Lorentzian ($n = 1$) and a pure Gaussian ($n = 2$). It should be emphasized, however, that there is no direct theoretical justification for the approximation of a Brereton function to a sum of a Weibullian and one or two exponential functions. This approximation is basically an empirical one.

5. Results and discussion

5.1. Structural characterization of the PE sample

Fig. 1 shows a proton decoupled ^{13}C NMR spectrum of a 12.5 wt.% of the PE sample dissolved in ODCB at 403 K with proton decoupling applied between successive 90° r.f.-pulses. The type of branch (Fig. 1) is identified according to a recent work by Hansen et al. [23] and reveals only butyl branches (4–5 per 1000 main chain carbons).

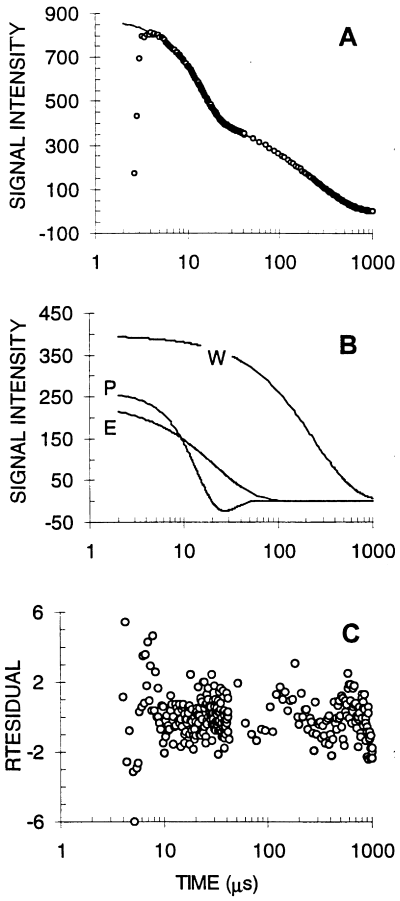

Fig. 2. (A) Corrected FID signal of a PE sample at $T = 386$ K. Solid curve represents model fit to a Pake–Weibullian-Exponential function (the PWE-model); (B) illustration of the different contribution to the FID, where *P*, *W* and *E* represent the Pake function, the Weibullian function and the single Exponential function, respectively; (C) residual between observed and calculated (PWE-model) FIDs.

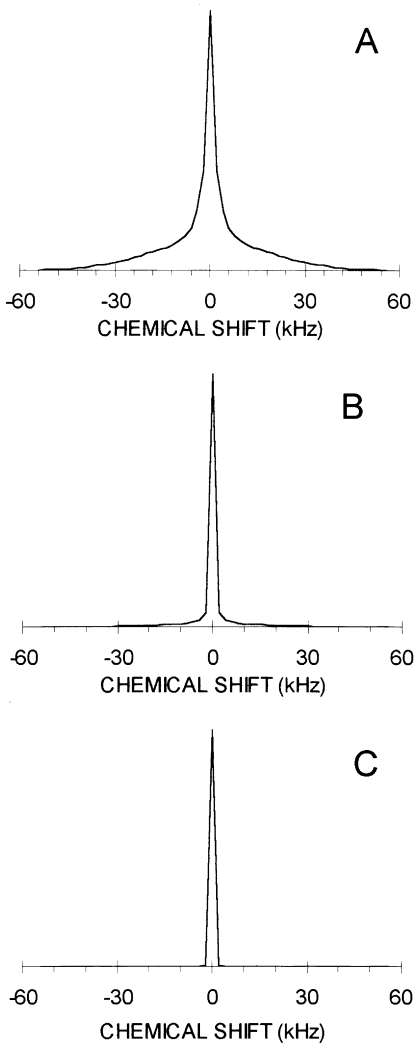

Fig. 4. Frequency spectra obtained by Fourier Transformation of model fitted FIDs of sample PE at (A) $T = 360$ K; (B) $T = 378$ K; and (C) $T = 396$ K, respectively.

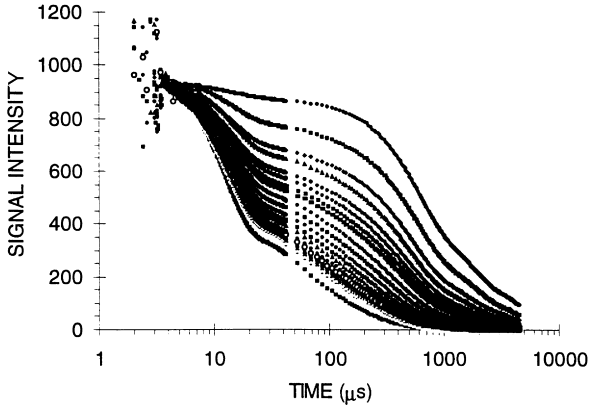

Fig. 3. Observed FIDs during heating of a pre-melted PE sample from 360 to 397 K. From top to bottom $T = 360$, 370, 372, 374, 376, 378, 380 382, 384, 386, 388, 390–397 K. See text for further details.

5.2. FID analysis of the PE sample

For times larger than 2 ms, all FIDs are well fitted by a single exponential function (Eq. (3), with $n = 1$), and will be discussed in the later section. This fitted function was subtracted from the observed FID, resulting in a new or "corrected" FID, as illustrated in Fig. 2(A) ($T = 386$ K). Note the significant distortion of the FID at the start of the acquisition, due to rf-pulse breakthrough. These initial data points ($t \leq 4$ μs) were excluded from the model fit. In a recent publication we showed that at room temperature a sum of a single Pake function, Eq. (1a), and a Brereton function could be well fitted to the observed FID of different PE samples [10]. In this work, the sum of a Brereton function and a Pake function was found to give a satisfactory representation of the FID only at low temperature ($T =$ 360–380 K). When increasing the temperature (<380 K), this model resulted in a significantly poorer fit. Thus, a model composed of a sum of one Pake function and two

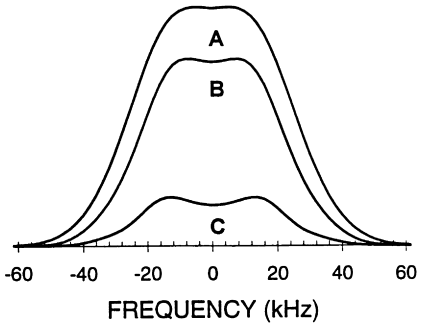

Fig. 5. Calculated frequency spectra of the crystalline phase of sample PE at the same temperatures as shown in Fig. 4. I.e., at (A) $T = 360$ K; (B) $T = 378$ K; and (C) $T = 396$ K. The spectra were obtained by Fourier Transformation of the Pake function contribution to the FIDs in Fig. 3.

Weibullian functions, Eq. (3), resulted in a much better fit to the observed FID within the whole temperature range investigated. This model fit is shown by the solid curve in Fig. 2(A). Fig. 2(B) illustrates the separate contributions from each of these functions, where P represents the Pake function (Eq. (1a)), W represents the Weibullian (Eq. (3)), and E represents a single exponential function (Eq. (3) with $n = 1$). The residual, i.e. the difference between the observed and the model fitted FIDs, is presented in Fig. 2(C) and suggests that the error is small and randomly distributed. This observation was found to be of genuine nature at all temperatures investigated, except at the two higher temperaures, in which the envelope of the residuals exposed a small, low-frequency oscillation. On this background, the

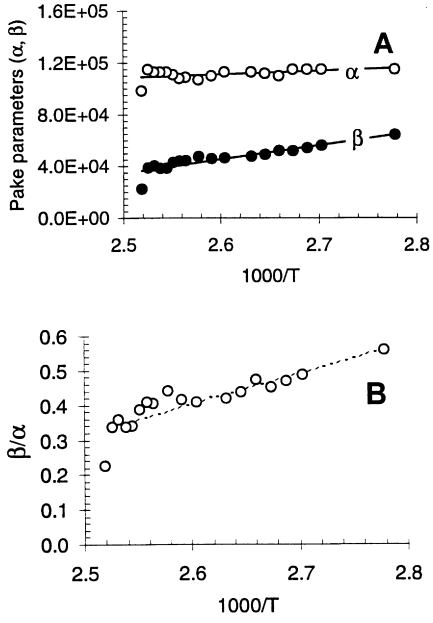

Fig. 6. (A) Pake parameters (α and β Eq. (1a)) versus temperature. These parameters were obtained by fitting a PWEE-model to the observed FIDs, as discussed in the text; (B) β/α-ratio versus temperature as obtained from the data in Fig. 6(A). The solid and dotted curves represent linear least square fits to the observed data.

Pake–Weibullian Exponential–Exponential ("PWEE") model was used throughout in this work. If replacing the Pake function by an Abragamian, Eq. (2), a slightly modified model ("AWEE") is obtained, which has been reported to give excellent fit to the FID of solid polypropylene [9]. However, the Abragamian is mainly a phenomenological expression, which yields little or no physical insight. This is in contrast to a Pake function. The replacement of a Pake function with an Abragamian results in a simpler and faster numerical approach, which gives a slightly poorer fit than the PWEE-model. We have implemented this latter model (AWEE) in the present work, mainly for comparative purposes.

The FIDs acquired at different temperatures are shown in Fig. 3 and demonstrate the systematic change in the shape of the FID versus temperature. This effect is better illustrated in Fig. 4, which shows the Fourier-Transformed (FT) spectra of the fitted FIDs at $T = 360$, 378 and 396 K, respectively. The corresponding frequency spectra of the crystalline phase (Pake function) are plotted in Fig. 5, and demonstrate clearly the significant reduction in signal intensity of this phase with increasing temperature. The shape of these spectra also changes with temperature and will be discussed in the next section.

5.3. Crystalline phase

The "FID analysis approach" applied in this work makes it possible to obtain detailed information regarding the different phases of the PE sample, in particular the crystalline phase. Eq. (1) shows that the line shape of the Pake function in the frequency domain depends on only two parameters, α and β. These parameters are plotted in Fig. 6(A) versus the inverse absolute temperature and show that α is nearly constant. The parameter β increases with decreasing temperature. Likewise, the α/β ratio increases with decreasing temperature, as shown in Fig. 6(B). The solid/dotted curves in Fig. 6 represent linear least squares fit to the observed data. According to the work of Pedersen [24], the doublet structure is less pronounced, in general, with increasing β/α-ratio from approximately 0.4. For $\beta/\alpha > 0.70$, the spectrum is without any fine structure as suggested by the frequency spectrum in Fig. 5(A). By defining the crystallinity of the sample as the signal intensity of the Pake function divided by the total signal intensity, the crystallinity versus temperature can be calculated. The results are shown in Fig. 7, suggesting the crystallinity to decrease approximately linearly with increasing temperature up to 392 K. Above this temperature the crystallinity drops markedly with increasing temperature. We tentatively interpret this abrupt change in crystallinity vs. temperature as the onset of melting.

It is worth noting that the experimentally determined proton–proton distance, as calculated from the observed α-value ($1.15 \times 10^5\,s^{-1}$), is equal to (1.69 ± 0.05) Å. This result is in excellent agreement with the value of

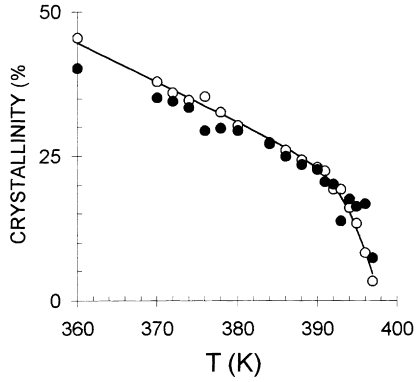

Fig. 7. Crystallinity versus temperature as determined by the PWEE-model fit (○) and the AWEE-model fit (●) to the observed FIDs in Fig. 3. The solid curve represents a model fit and is discussed in the text.

1.7 Å, as determined by X-ray measurements, and is the main reason for adopting the Pake function approach. However, one point of concern, is that the calculated distance 2α between the two symmetric "peaks" of the Pake function ($2\alpha = 2.3 \times 10^5\ s^{-1} \equiv 37$ kHz) is less than the width estimated from the frequency spectra of PE (≈50 kHz) in reference [25]. Keeping in mind the uncertainty of 5–10% in the derived α-value, the actual width of the Pake function in this work may be as high as 42 kHz. However, the smaller line width determined from the simple Pake model approach may originate from the exclusion of asymmetry broadening effects. The nature of this assymmetry can often be interpreted in terms of the relative angular position of nearby interacting pairs of protons in the crystal chain [26]. Thus, the simple Pake function is not an exact expression for PE, but must be treated as a reasonable approximation.

If replacing the Pake function by an Abragamian in the model fit, no significant difference in crystallinity can be inferred (Fig. 7). The solid curve represents model calculation and will be discussed in a later section. These results give support for the compatibility and consistency between the two models (PWEE and AWEE). The two parameters, ω_0 and T_2*, which uniquely define the Abragamian (Eq. (2)), are plotted versus temperature in Fig. 8. They will be used to

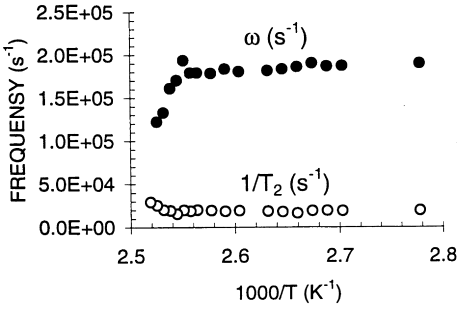

Fig. 8. Frequency parameters, ω and $1/T_2$, of the Abragamian function, Eq. (2), as obtained by model fit (AWEE-model) to the observed FID in Fig. 3.

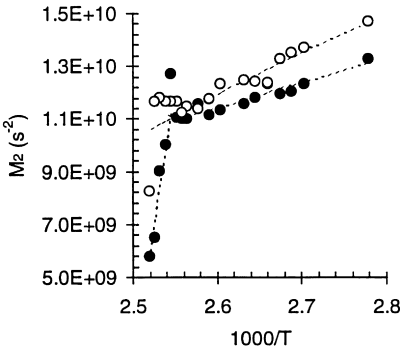

Fig. 9. Second moment (M_2) of the crystalline part of the FID versus inverse absolute temperature. The second moment is calculated from Eq. (4), using two different models, the PWEE-model (○) and the AWEE-model (●). The dashed curves represent model fits to Eq. (7). See text for further details.

derive the second moment, M_2, as described in the next section.

We can expand the Pake function and the Abragamian in Taylor series of time (t)

$$F = 1 - \frac{1}{2!}M_2t^2 + \frac{1}{4!}M_4t^4 + \cdots + \frac{1}{(2n)!}M_{2n}t^{2n} + \cdots, \tag{4a}$$

where

$$M_{2,\mathrm{Pake}} = \frac{4}{5}\alpha^2 + \beta^2 \tag{4b}$$

and

$$M_{2,\mathrm{Abragam}} = \frac{2}{T_2^2} + \frac{\omega^2}{3}. \tag{4c}$$

Here M_2 is the second moment, M_4 is the fourth moment, etc. The second moment versus inverse temperature is shown in Fig. 9 for both models (the "PWEE-model" and the "AWEE-model"). The dotted/solid curves represent model fits and will be commented on in a later section. A small, but significant difference in M_2 between the two models can be inferred. However, both second moments show an approximate linear decrease with increasing temperature until the onset of melting, at which temperature the second moment falls off dramatically. In the discussion that follows we will use the data obtained from the Pake function analysis (PWEE-model) due to its improved physical relevance and better theoretical fundament, as compared to the Abragamian. From the data presented in Fig. 8, the second moment of the Abragamian is basically determined by the frequency factor, ω. The spin–spin relaxation rate, $1/T_2$, shows only a minor influence on the second moment.

According to an approach discussed by English et al. on spatial averaging [27], the molecular motion is reflected by the part of the second moment that is modulated by the motion on the time scale of the measurement in question. If the symmetry of the motion is such that the molecular interaction vector, r, samples orientations (ϕ) which have

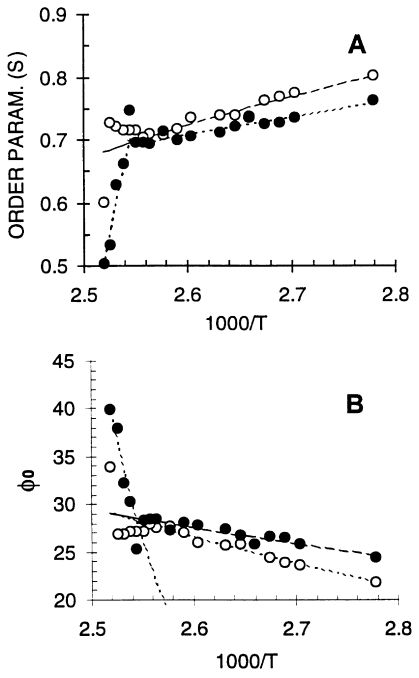

Fig. 10. (A) order parameter, S_β (Eq. (5)), and (B) standard deviation of a Gaussian distribution of small-angle vibrations (β_0; Eq. (6)) of the crystalline phase versus inverse absolute temperature (1000/T), as calculated from the two different models, the PWEE-model (○) and the AWEE-model (●). The dashed curves in (B) were determined by straight-line fits to the observed data. The dashed curves in (A) were calculated from Eq. (6) by implementing the linear relation between β_0 versus 1000/T in (B). See text for further details.

an axially symmetric distribution about a direction, d, then

$$S_\phi^2 = \frac{1}{2}(3\cos^2\phi - 1) = \frac{M_2}{M_2^0}, \tag{5}$$

where $S_\phi$defines the order parameter, i.e. the ratio between the observed second moment (M_2) and the static second moment ($M_2^0 = 2.28 \times 10^{10}\ \mathrm{s}^{-2}$)[10]. As the orientational angle is not expected to be the same for all parts of the polymer chain, we will assume that it can be described by a distribution of angles. Assuming the distribution to be random, a Gaussian function with a standard deviation, ϕ_0, may be used, giving [27]

$$S_\phi = \frac{1}{2}\frac{\int_0^{2\pi}(3\cos^2\phi - 1)\exp(-(\phi/\sqrt{2}\phi_0)^2)\,\mathrm{d}\phi}{\int_0^{2\pi}\exp[-(\phi/\sqrt{2}\phi_0)^2]\,\mathrm{d}\phi}. \tag{6}$$

Fig. 10 shows S_ϕ and ϕ_0 versus temperature and are in excellent agreement with corresponding analysis reported on semi-crystalline PE terphtalate [27]. Also, the "activation energy" was found to be of the same order of magnitude, 9 kJ/mol. Using the Abragamian second moment, resulted in a somewhat smaller activation energy of 5 kJ/mol. Typically, ϕ_0 increases linearly with increasing temperature up to $T = 392$ K, above which temperature ϕ_0 increases substantially, and is tentatively explained by the onset of melting. The ϕ_0 versus temperature data presented in Fig. 10(B) are well fitted by straight lines for temperatures $T < 392$ K. These empirical fits are used to recalculate the order parameter S_ϕ from Eq. (6). The results are shown by the dashed curves in Fig. 10(A).

Another observation, which needs some attention, is the levelling off of the second moment within a small temperature region of approximately 5 K and close to the onset of melting (PWEE-model, Fig. 9). A similar observation has been reported by Olf et al. [28,29] back in 1970 on an investigation of oriented mats of PE single crystals. The second moment variation with temperature of a powder average PE sample, as calculated from such oriented mat samples [28], is in agreement with the corresponding second moment of the crystalline phase observed in this work. A similar leveling off of the second moment derived from application of the AWEE-model (Fig. 9), cannot be recognized as easily. These results give support to the conclusion that the Pake function gives a physically reliable description of the crystalline phase within semi-crystalline PE samples. This statement is also sustained by previous NMR measurements [10].

To decide what type of motion that dominates the α-process within the crystalline phase, we recognize from the temperature variation of the second moment, that the intra-molecular contribution (α in Eq. (1)) is nearly constant and temperature independent. Only the inter-molecular contribution (β in Eq. (1)) to the second moment varies significantly with temperature, suggesting that the motional process is basically an inter-molecular one (Fig. 6(A)). This implies that the inter-nuclear vector, joining two protons on the same methylene unit, must have the same direction with respect to the external magnetic field during the motional process. Also, the magnitude of this same vector must remain practically constant in time. These constraints exclude the: (a) "flip-flop" motion, which consists of a rotational jump of the molecule around its axis by 180°, and a simultaneous translation along this axis by one CH_2-group, and (b) the incoherent rotational oscillations of the chains about their equilibrium positions in the crystal lattice [28,29]. We are then left with a molecular motion that may be described by a parallel displacement of the planar zig-zag segments of PE, perpendicular to their axes [28,29]. The overall change in the second moment from 325 to 392 K (α-process) is approximately $0.57 \times 10^{10}\ \mathrm{s}^{-2}$, corresponding to approximately eight gauss [2]. This is of the same order of magnitude as observed by Olf et al. [28,29] of approximately seven gauss [2].

The question remains on how to obtain information regarding the correlation time of the aforementioned molecular motion. We have used the most commonly applied method of Bloembergen, Purcell and Pound (BPP) [30]. In its most simple form, the motional correlation time τ is

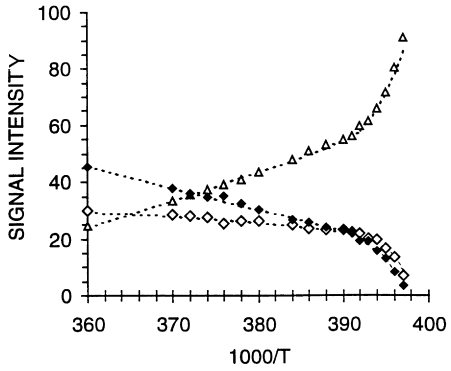

Fig. 11. Observed signal intensities of the crystalline C (◆), intermediate (◇) and amorphous A-phase of PE as a function of temperature (T). The dotted curves represent model calculations (Eq. (10)). See text for further details.

related to the second moment by

$$\tau = \frac{\lambda}{\sqrt{M_2}} \tan\left[\frac{\pi}{2}\frac{M_2}{M_2^0}\right], \tag{7}$$

where $M_2^0 (= 2.28 \times 10^{10}\ \mathrm{s}^{-2})$ is the limiting, rigid-lattice second moment and λ is a constant of the order of unity. Its value will depend on the shape of the resonance peak. We have chosen $\lambda = \sqrt{8\ln 2}$, in accordance with the work of Kubo and Tomita and others [31–34]. Assuming the motional process to be thermally activated, in which the correlation time, τ, can be described by an Arrhenius equation

$$1/\tau = P \exp\left(-\frac{\Delta E}{RT}\right) \tag{8}$$

where (ΔE) is the activation energy, T the absolute temperature, and P is the pre-exponential factor (the attempt frequency). These parameters can be determined by inserting Eq. (8) into (7) and fitting this combined equation to the observed second moment (M_2) versus inverse absolute temperature ($1000/T < 2.54$) by a non-linear least squares technique. The results are shown by the dashed curves in Fig. 9, with $P = 9.34 \times 10^6\ \mathrm{s}^{-1}$ and $\Delta E = 13.5$ kJ/mol. The model fit predicts a correlation time of 17 μs at the onset of the α-process ($T = 323$ K) and a correlation time of 6.8 μs at the end of the α-process (or the onset of melting at $T = 393$ K), respectively. The straight, dashed line in Fig. 9 for $1000/T < 2.54$ is determined by a simple linear fit and has no physical significance. From dynamic mechanical experiments, this activation energy is more like 120 kJ/mol. The reason for this significant discrepancy is not understood, but suggests that NMR and dynamic mechanical experiments probe different molecular motions.

It is worth mentioning that the limiting, and minimum observable spin–spin relaxation time can be approximated by $\sqrt{M_2^0}$, which equals approximately 7 μs. Correlation times much larger than 7 μs can thus not be resolved or unravelled by spin–spin relaxation time measurements. In this case one should resort to spin–lattice relaxation time measurements. This particular method to probe molecular motion may, however, be complicated by spin diffusion effects [35,36], a topic which is outside the scope of this work.

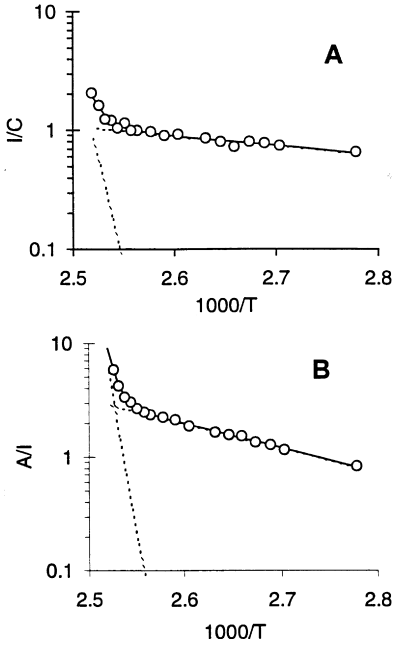

Fig. 12. Observed signal intensity ratios (R_i) versus inverse absolute temperature ($1000/T$) for (A) $R_1 = N_I/N_C$ and (B) $R_2 = N_A/N_I$. N_x represents the signal intensity of phase $X(= \mathrm{C, I, A})$. The dotted and solid curves represent model fits to Eq. (9). See text for further details.

5.4. Phase-equilibrium

A total of four separable FID-components can be extracted from model fitting to the observed FID. Three of these components, ascribed to the non-crystalline phases, are represented by capital letters: I, A_1 and A_2. The signal intensity versus temperature of the four FID-components are depicted in Fig. 11 and show a linear decrease with increasing temperature of both the crystalline signal intensity (C) and the I-signal intensity, up to approximately 393 K. At higher temperatures, the slope of the same two signal intensities versus temperature becomes much steeper. As already mentioned, this change in slope with temperature is tentatively identified as the onset of melting.

As shown by Brereton et al. [22] the FID of the amorphous phase (even in the melt) cannot be characterized by a single T_2 relaxation time, but rather by a multiple exponential decay. On this grounds, we have assigned the two signal components A_1 and A_2 to the amorphous phase. The signal intensity of the amorphous phase (A) is thus defined as the sum of signal intensities of the two components A_1 and A_2. As the NMR signal intensity (S) is directly proportional to the amount of polymer (N_S), a plot of the signal intensity

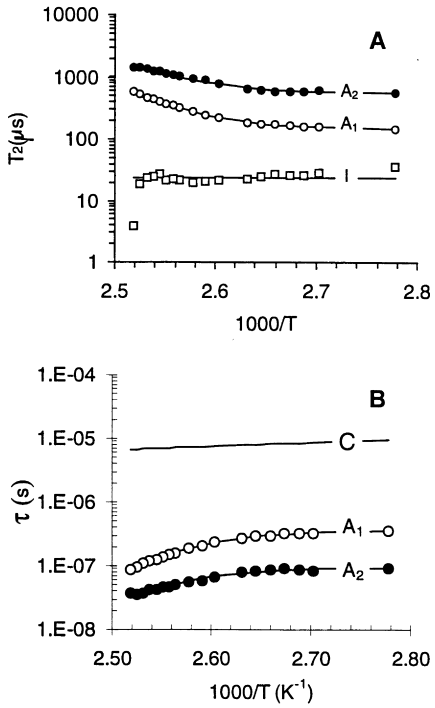

Fig. 13. (A) spin–spin relaxation time (T_2) versus inverse absolute temperature of the intermediate phase (I) and the amorphous phase-A (A_1 and A_2-components) as derived from a PWEE-model fit to the observed FIDs. The T_2 of phase I is determined from the AWEE-model fit. The solid curves of components A_1 and A_2 are calculated from Eq. (12) by applying the results obtained in Fig. 13(A); (B) correlation time, τ, versus inverse absolute temperature of components A_1 and A_2 (amorphous phase) as derived from Eq. (12). The solid curves are obtained by model fits to Eqs. (8) and (13).

ratios (R_i) against the inverse temperature ($1/T$) are shown in Fig. 12 for $R_1 = N_I/N_C$, $R_2 = N_A/N_I$. Within the whole temperature region investigated, these ratios can be well approximated by the following type of function:

$$R_i = a_{i1} \exp\left(-\frac{\Delta G_{i1}}{RT}\right) + a_{i2} \exp\left[-\frac{\Delta G_{i2}}{RT}\right], \tag{9a}$$

where a_{ij} and ΔG_{ij} (for $i = 1,2$) are constants. The observed and fitted R_i-values versus temperature are shown in Fig. 12, and reveal an abrupt change at a temperature corresponding approximately to the onset of melting. Within the α-process regime ($T > 393$ K), the observed ratios can be well approximated by the second term in Eq. (9a), i.e.

$$R_i = a_{i2} \exp\left[-\frac{\Delta G_{i2}}{RT}\right]. \tag{9b}$$

The results are indicated by the dotted curves in Fig. 12. The energy parameters ΔG_{i2}, within the α-regime, were found to be $\Delta G_{12} = (15.6 \pm 1.8)$ kJ/mol, $\Delta G_{22} = (40.9 \pm 2.1)$ kJ/mol.

The aforementioned results can be quantitatively rationalized, according to the following phase-equilibrium reactions:

$$C \overset{K_1}{\leftrightarrows} I \overset{K_2}{\leftrightarrows} A, \tag{10}$$

where the "equilibrium" constants K_i in Eq. (10) can be identified with the R_i-ratios discussed above. As matter is conserved, the total contribution of polymer from the respective phases, C, I, A must be constant, i.e.

$$N_C + N_I + N_A = \text{constant}. \tag{11}$$

If the constant in Eq. (11) is set equal to 100, the amount of polymer contributing to each phase can be calculated from the phase-equilibrium reaction, Eq. (10). The results are depicted as dashed curves in Fig. 11, and are in quantitative agreement with observation. The solid curve in Fig. 7 is calculated from this same phase-equilibrium model, Eq. (10), We tentatively assign the four different phases to the crystalline phase (C), the intermediate phase (I), and the amorphous phase (A), respectively. This assignment of phases will be discussed in more details in the next section, when trying to pin down the molecular motional characteristics of the polymer in question.

5.5. Non-crystalline phases

The separate FID components of the three phases, I, A_1 and A_2 can be described by single exponential functions in the temperature range $T = 360$–392 K. In the narrow temperature region $T = 392$–397 K, the FID of the A_2 component changes continuously from a pure Exponential to a pure Gaussian shape, indicating that this phase may be characterized by a distribution of spin–spin relaxation times rather than a single relaxation time. The other two FID-components decay exponentially in the whole temperature range investigated. The exact reason for the change in shape of the FID-component A_2 is not well understood, but may originate from spin-diffusion effects between phases [35,36]. This predicament is, however, outside the scope of this work, and needs further investigation.

The spin–spin relaxation times versus temperature of the three components I, A_1 and A_2 are plotted in Fig. 13(A) and are distinctly different. The relaxation time of the I-component is practically independent of temperature and equals $T_2 = (23.6 \pm 2.9$ μs). This is the same relaxation time ($T_2 = (21.4 \pm 0.95)$ μs) as found in the crystalline phase (C) when assuming the crystalline FID to be described by an Abragamian function (AWEE-model). It needs to be emphasized, however, that the Abragamian function has little or no physical relevance, making this derived T_2 relaxation time somewhat dubious. At least, the T_2 obtained by this model fit is somewhat ambiguous.

However, the shape of the crystalline FID, whether it is defined by an Abragamian function (AWEE-model) or a Pake function (PWEE-model), is rather different from an exponential FID (I-component) and are therefore not immediately comparable. This basic difference in FID shape between the C-component and the I-component,

suggests that these components (I and C) must be of different nature.

The next question concerns how to extract information regarding the molecular motion from the T_2 data in Fig. 13(A). One approach is to apply Eq. (12) [31–34], which represents a modified version of Eq. (7).

$$\frac{\tau}{T_2} = \lambda \tan\left[\frac{\pi}{2}\frac{1/T_2^2}{M_2^0}\right]. \tag{12}$$

This equation identifies the molecular motion by a correlation time τ. In particular, this equation predicts a limiting value of the spin–spin relaxation time equal to $\sqrt{M_2^0}$ when the correlation time approaches infinity. Recalling that the spin–spin relaxation time of the I-component (Fig. 13(A)) is approximately independent of temperature may suggest that the molecular motion is located within the long correlation time regime. This makes it difficult if not impossible to derive reliable molecular motional information (correlation time) from spin–spin relaxation time measurements.

One way to overcome this problem is to perform spin–lattice relaxation time measurements. Although this approach is complicated by spin-diffusion effects, it can be solved [35,36].

Fig. 13(B) shows the correlation time versus temperature of the A_1 and A_2-components of the amorphous phase (A) as calculated from Eq. (12). As can be inferred from this figure, the correlation time cannot be assigned to a simple Arrhenius behavior as defined by Eq. (8).

To further rationalize this behavior we may introduce a distribution of correlation times. However, the simplest dynamical model to be invoked is a "parallel-τ" model [37,38], which takes the form

$$\frac{1}{\tau} = \frac{1}{\tau_A} + \frac{1}{\tau_B}. \tag{13}$$

The individual correlation times τ_A and τ_B are assumed to be independent, thermally activated, and thus described by Eq. (8).

The solid curves in Fig. 13(B) represent linear least squares fits of Eq. (13) (combined with Eq. (8)) to the observed correlation time data. Although the activation energy of the "A-process" could not be reliably estimated, it is shown to be rather small ($\backsim$0 kJ/mol) for both phases. However, the activation energy of the "B-process" is significantly larger and approximately 160 kJ/mole for both the amorphous components. The data reveal a faster molecular motion of the "A_2-component" compared to the "A_1-component" at all temperatures. These results support the non-homogenous molecular motional characteristics of the amorphous phase as suggested earlier by Brereton [21,23]. For comparison, the correlation time characterizing the molecular motion within the crystalline phase, as calculated from Eq. (7), is plotted on the same figure.

The molecular motional characteristics illustrated in Fig. 13(B) were used to identify the three phases within the polymer sample, i.e. C (crystalline phase), I (intermediate phase) and A (amorphous phase).

6. Conclusion

The observed FID of a pre-melted PE sample is shown to be decomposed into four separate time signals, at all temperatures investigated (360–397 K). The four time signals are derived by fitting two different models, the "Pake–Weibullian Exponential–Exponential (PWEE) model" and the "Abragamian–Weibullian-Exponential–Exponential (AWEE) model"—to the observed FID.

Analysis of the derived spin–spin relaxation times and/or second moments makes it possible to extract motional characteristics, which in turn enables the different signals to be assigned to a crystalline phase (C), an intermediate phase (I) and an amorphous phase (A; composed of two components A_1 and A_2). The relative variation in intensity versus temperature of the three phases can be rationalized according to a phase-equilibrium model: C $\rightleftarrows$ I $\rightleftarrows$ A.

Both models (PWEE and AWEE) predict—within experimental error—the same temperature variation of the different phases. However, the two models result in small but significant differences in the derived crystalline phase second moments. As the Abragamian function in the AWEE-model lacks physical significance, we strongly believe that the Pake function in the PWEE-model gives a better description of the crystalline phase of the PE sample. Also, the latter model gives, generally, a somewhat better fit to the observed FID. The PWEE-model suggests that molecular motion within the crystalline phase may be described by a parallel displacement of the planar zig-zag segments, perpendicular to their axes.

Acknowledgements

We are grateful to Borealis AS for making the PE samples available for NMR characterization.

References

[1] Kitamaru R, Horri F, Murayama K. Macromolecules 1986;19:636.
[2] Kitamaru R, Horii F, Zhu Q, Basset DC, Olley RH. Polymer 1994;35:1171.
[3] Bruckner S, Meille SV, Sozzani P, Torri G. Makromol Chem, Rapid Comm 1990;11:55.
[4] Bunn A, Cudby EA, Harris RK, Packer KJ, Say BJ. Polymer 1982;23:694.
[5] VanderHart DL. J Magn Res 1981;44:117.
[6] Gomez MA, Tanaka H, Tonelli AE. Polymer 1987;28:2227.
[7] Fleming WW, Fyfe CA, Kendrick RD, Lyerla JR, Vanning H, Yannoni CS. In: Woodward AE, Bovey FA, editors. Polymer characterization by ESR and NMR, 142. Washington, DC: American Chemical Society, 1980. p. 212.
[8] Packer KJ, Pope JM, Yeung RR, Cudby EA. J Pol Sci, Pol Phys Ed 1984;22:589.

[9] Dadayli D, Harris RK, Kenwright AM, Say BJ, SünnetÇioğlu MM. Polymer 1994;35:4083.
[10] Hansen EW, Kristiansen PE, Pedersen B. Polymer 1998, in press.
[11] Boyd RH. Polymer 1985;26:323–47.
[12] Bassett DC. Principles of polymer morphology. Solid state science series. Cambridge, New York: Cambridge University Press, 1981.
[13] Chen Q, Yamada T, Kurosu H, Ando I, Shinono T, Doi Y. J Mol Struct 1991;263:319.
[14] Ando I, Yamanobe T, Akiyama S, Komoto T. Solid State Comm 1997;62:785–8.
[15] Förster H. Bruker (private communication).
[16] Pake GE. J Chem Phys 1948;16:327.
[17] Engelsberg M, Lowe IJ. Phys Rev 1974;10:822.
[18] Look DC, Lowe IJ, Northby JA. J Chem Phys 1966;44:3441.
[19] Abramowitz, Stegun I. Handbook of mathematical functions. New York: Dover, 1970. p. 300.
[20] Abragam A. Principles of nuclear magnetism. Oxford: Oxford University Press, 1961. p. 120.
[21] Brereton MG. J Chem Phys 1991;94:2136.
[22] Brereton MG, Arden IM, Boden N, Wright P. Macromolecules 1991;24:2068.
[23] Hansen EW, Blom R, Bade OM. Polymer 1997;38:4295.
[24] Pedersen B. Acta Chem Scand 1968;22:444.
[25] Packer KJ, Pope JM, Yeung RR. J Pol Science: Pol Phys Ed 1984;22:589.
[26] Holcomb DF, Pedersen B. J Chem Phys 1963;38:54.
[27] English AD. Macromol 1984;17:2182.
[28] Olf HG, Peterlin A. J Pol Sci; Part A-2 1970;8:753.
[29] Olf HG, Peterlin A. J Pol Sci; Part A-2 1970;8:771.
[30] Bloembergen N, Purcell EM, Pound RV. Phys Rev 1948;73:679.
[31] Kubo R, Tomita K. J Phys Soc, Jpn 1954;9:888.
[32] Waugh JS, Fedin EI. Sov Phys Solid State 1963;3:1633.
[33] Resing HA. J Chem Phys 1965;43:669.
[34] Gran HChr, Hansen EW, Pedersen B. Acta Chem Scand 1997; 51:24.
[35] Packer KJ, Poplett IJF, Taylor MJ, Vickers ME, Whittaker AK, Williams KPJ. Makromol Chem Makromol Symp 1990;34:161.
[36] Colquhoun IJ, Packer KJ. Br Polym J 1987;19:151.
[37] Barnaal D, Kopp M, Lowe IJ. J Chem Phys 1976;65:5495.
[38] Barnaal D, Slotfeldt-Ellingsen D. J Phys Chem 1983;87:4321.